

A Journal of the Gesellschaft Deutscher Chemiker

# Angewandte Chemie

GDCh

International Edition

[www.angewandte.org](http://www.angewandte.org)

## Accepted Article

**Title:** Exotic compositional ordering in Mn-Ni-As intermetallics

**Authors:** Bruno Gonano, Øystein Slagtern Fjellvåg, Gwaldys Steciuk, Dipankar Saha, Denis Pelloquin, and Helmer Fjellvåg

This manuscript has been accepted after peer review and appears as an Accepted Article online prior to editing, proofing, and formal publication of the final Version of Record (VoR). This work is currently citable by using the Digital Object Identifier (DOI) given below. The VoR will be published online in Early View as soon as possible and may be different to this Accepted Article as a result of editing. Readers should obtain the VoR from the journal website shown below when it is published to ensure accuracy of information. The authors are responsible for the content of this Accepted Article.

**To be cited as:** *Angew. Chem. Int. Ed.* 10.1002/anie.202006135

**Link to VoR:** <https://doi.org/10.1002/anie.202006135>

## COMMUNICATION

## Exotic compositional ordering in Mn-Ni-As intermetallics

Bruno Gonano<sup>a</sup>, Øystein Slagtern Fjellvåg<sup>b</sup>, Gwladys Steciuk<sup>c</sup>, Dipankar Saha<sup>a</sup>, Denis Pelloquin<sup>d</sup> and Helmer Fjellvåg<sup>\*a</sup><sup>a</sup>Center for Materials Science and Nanotechnology, Department of Chemistry, University of Oslo, P.O. Box 1033 Blindern, N-0315 Oslo, Norway<sup>b</sup>Department for Neutron Materials Characterization, Institute for Energy Technology, PO Box 40, NO-2027, Kjeller, Norway.<sup>c</sup>Institute of Physics, Academy of Sciences of the Czech Republic, v.v.i, Na Slovance 2, Prague 18221, Czech Republic<sup>d</sup>Laboratoire CRISMAT, UMR 6508 CNRS ENSICAEN, 6 bd du Maréchal Juin, 14050 Caen Cedex 4, France

**Abstract:** In this work we benefited from recent advances in tools for crystal structure analysis that enabled us to describe an exotic nanoscale phenomenon in structural chemistry. The  $\text{Mn}_{0.60}\text{Ni}_{0.40}\text{As}$  sample of the  $\text{Mn}_{1-x}\text{Ni}_x\text{As}$  solid solution, exhibits an incommensurate compositional modulation intimately coupled with positional modulations. The average structure is of the simple NiAs type, but in contrast to a normal solid solution, we observe that manganese and nickel segregate periodically at the nano-level into ordered MnAs and NiAs layers with thickness of 2-4 face-shared octahedra. The detailed description was obtained by combination of 3D electron diffraction, scanning transmission electron microscopy and neutron diffraction. The distribution of the manganese and nickel layers is perfectly described by a modulation vector  $q = 0.360(3) c^*$ . Displacive modulations are observed for all elements as a consequence of the occupational modulation, and as a means to achieve acceptable Ni-As and Mn-As distances. This extraordinary modulated evolution of magnetic MnAs and non-magnetic NiAs-layers with periodicity at  $\sim 10 \text{ \AA}$  level, may provide an avenue for spintronics.

## Introduction

Since the discovery of X-rays, scientists have studied atomic arrangements in solids considering their intrinsic beauty and their role as the active link between atoms and physical properties of materials. In a crystal structure, one finds different sites for cations and anions, reflecting their different chemical properties (*i.e.* size, charge, electronegativity, *etc.*). This gives rise to a huge range of crystal structure types, from simple to very complex ones among proteins, organic and inorganic compounds.

Incommensurately modulated crystal structures with their high complexity, attract a lot of interest in solid-state science. Both occupancy and position can be modulated. The modulation can originate from a wide variety of structural perturbations like incommensurate oxygen vacancies ordering<sup>[1]</sup>, polyhedral distortions<sup>[2,3]</sup> and compositional ordering<sup>[4]</sup>. Incommensurate modulations are quite well understood in oxides while intermetallics present a challenge in terms of structural analysis<sup>[5-7]</sup>.

An incommensurate, partial cation occupancy modulation has been reported for  $\text{LaNb}_{0.88}\text{W}_{0.12}\text{O}_{4.06}$ <sup>[8]</sup>. This compound has a modulation linked to a preferential cation nano-segregation of tungsten atoms. In intermetallics, positional modulation has been observed in different compounds, *e.g.* in the Nowotny Chimney-ladder phases<sup>[9-11]</sup>, that can be described as an intertwining between two sublattices. Similar phenomena are present in  $\text{Cu}_{3+x}\text{Si}$ <sup>[12]</sup>, which displays a very complex incommensurate modulation and illustrate well the complexity in disclosing structural details for such systems.

Ferromagnetic MnAs (space group  $P6_3/mmc$ ) is an example of a simple crystal structure derived from ABAB sphere packing of As, with Mn in octahedral sites formed by closed-packed As-layers,

giving rise to face-sharing chains of  $\text{MnAs}_6$ -octahedra along [001] with two octahedra per unit cell. In the *ab*-plane, the  $\text{MnAs}_6$ -octahedra are edge-sharing. Pauli paramagnetic NiAs (space group  $P6_3/mmc$ ) adopts the same structure type, but with different unit cell parameters (due to the different size of Mn and Ni).

The intermediate solid solution between MnAs and NiAs,  $\text{Mn}_{1-x}\text{Ni}_x\text{As}$  ( $0 \leq x \leq 1$ ), was investigated in the 1980s and revealed an unsolved structural phenomenon for  $0.25 \leq x \leq 0.75$ <sup>[13]</sup>. A possible modulation due to Ni ordering was proposed, but no available technique could confirm or invalidate this speculation. Therefore, the question of a Mn-Ni-ordering in  $\text{Mn}_{1-x}\text{Ni}_x\text{As}$  remained unanswered. Today, state-of-the-art analytical tools have evolved to the point that revisiting this system can provide answers. We here reveal an exotic Mn-Ni-ordering in  $\text{Mn}_{0.60}\text{Ni}_{0.40}\text{As}$ , which appears to represent a phenomenon not earlier observed.

## Results and Discussion

Initially, we studied the lattice of  $\text{Mn}_{0.60}\text{Ni}_{0.40}\text{As}$  by conventional electron diffraction (ED), and the data revealed an expected complex unit cell. Electron diffraction pattern of the [100]-zone axis shows additional reflections (**Fig. 1a**) that can be indexed by an incommensurate modulation vector ( $q = 0.36 c^*$ ), confirming the presence of additional order in the compound. The corresponding High-Angle Annular Dark Field (HAADF) image coupled with local EDX collections yields good elemental contrasts correlated to Mn and Ni species and reveals two types of layers perpendicular to the modulation vector [001] (**Fig. 1b and c**). We interpret these images as a specific ordering between Mn and Ni based layers, as supported by energy-dispersive X-ray spectroscopy mapping (EDX) (**Fig. 1b**).

The thickness of these layers can be measured in terms of the number of connected octahedra, being 3-4 for the MnAs and 2-3 for the NiAs slabs of the integrated structure. This creates a unique nanolayered structure, with the compositional modulation being a genuine part of the crystal structure of the phase. We note that the layers appear to be fully occupied by either Mn or Ni, indicating that the ordering is complete.

Careful analysis of the As-As distances along [001] in the x25M HAADF image, reveals a distinct difference between the zones richer in Mn or in Ni (**Fig. 1c**). Whereas for the brighter layer (Ni-rich) the As-As distance tends to be shorter, it increases in the darker Mn-rich regions, according to the longer *c*-axis of MnAs (5.8 Å) compared to that of NiAs (5.0 Å). This is supported by the extracted line profile for the As-As distances in **Fig. 1d**.

At this point, it is clear that the Mn-Ni ordering is real. We now use 3D ED to unveil a structural model.<sup>[14]</sup> This technique has recently proved his ability to yield valid structural models in complex systems<sup>[15]</sup> and provide single-crystal diffraction data on small areas of few hundreds of nanometers, also on powder samples. It must be mentioned here that 3D ED represents a broad range of experimental protocols and that this study refers to Precession Electron Diffraction Tomography (PEDT).

## COMMUNICATION

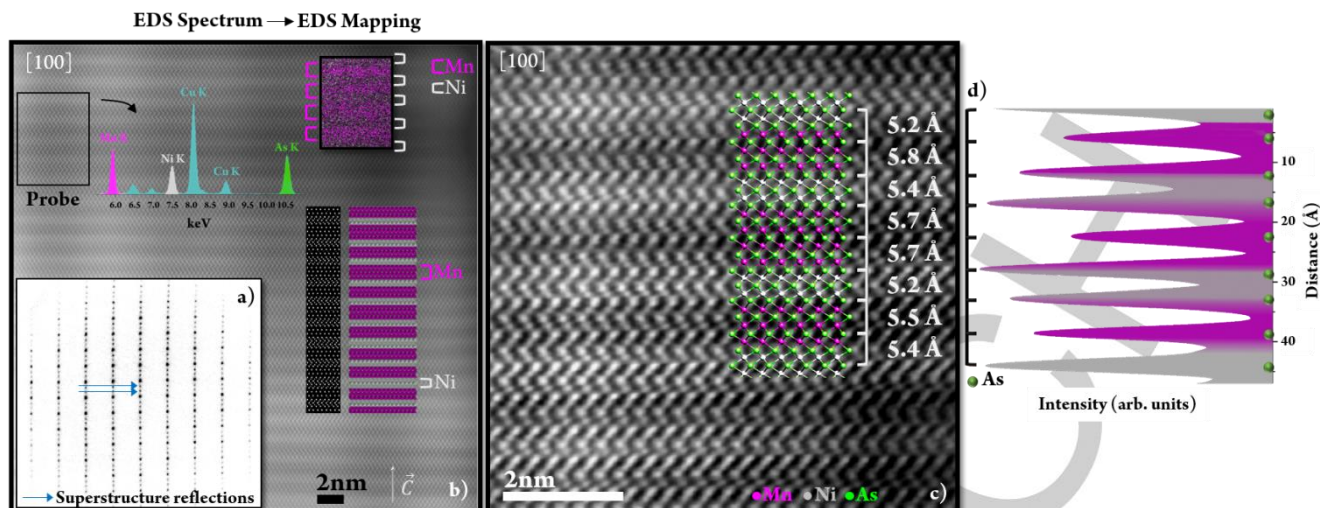


**Figure 1:** a) Electron diffraction of the [100]-zone axis of  $\text{Mn}_{0.60}\text{Ni}_{0.40}\text{As}$  showing satellite reflections, corresponding to an incommensurate modulation vector along  $c^*$  ( $q = 0.36 c^*$ ); b) Experimental [100] HAADF image of  $\text{Mn}_{0.60}\text{Ni}_{0.4}\text{As}$  (magnification  $\times 8\text{M}$ ). Bright dots are related to As rows while darker and brighter layers represent MnAs and NiAs, respectively. On the right side, simulated image confirms the goodness of the structural model. Latter is inserted beside. Top left inset: EDS spectrum related to recorded zone (Probe) identified by a black box. Top right inset: EDS mapping evidencing richer zones in Mn (purple) and Ni (grey); c) Experimental [100] HAADF image of  $\text{Mn}_{0.60}\text{Ni}_{0.4}\text{As}$  (magnification  $\times 25\text{M}$ ) showing variations in distances between As atoms from Mn (darker) and Ni (brighter) layers. A snapshot of the structural model is inserted; d) Intensity line profile extracted from the HAADF image along [001], displaying the variations of As-As distances in the MnAs and NiAs layers.

3D ED shows the expected hexagonal subcell, but also additional reflections at incommensurate positions (**Fig. 2a**). The reciprocal space was indexed using the superspace formalism considering a hexagonal unit cell:  $a = 3.653(8) \text{ \AA}$ ,  $c = 5.417(3) \text{ \AA}$  and with a modulation vector  $\mathbf{q} = 0.360(3) c^*$  to index satellite reflections up to first order. As expected from the conventional ED, the modulation is incommensurate. The volume of the average unit cell ( $V = 62.67 \text{ \AA}^3$ ) is in between the volumes of NiAs ( $V = 56.7 \text{ \AA}^3$ ) and MnAs ( $V = 68.55 \text{ \AA}^3$ ).<sup>[16],[17]</sup> Information on symmetry is obtained from e.g. the sections  $11lm$  and  $0klm$  of the reciprocal space for which the extinction conditions  $l = 2n$  on  $00l$  and  $11lm$  are characteristic of a  $6_3$ -screw axis along [001] and a  $c$ -glide mirror perpendicular to [1-10], respectively (**Fig. 2b**). These conditions are compatible with two superspace groups (SSG);  $P6_3/mmc(00\gamma)0000$  and  $P6_3mc(00\gamma)000$ . The structure was solved from the 3D ED data in SSG  $P6_3/mmc(00\gamma)0000$  with  $\mathbf{q} = 0.360(3) c^*$  and a data coverage of 100% for  $0.7 \text{ \AA}^{-1}$  resolution shell. Our subsequent refinements indicated that the structure is centrosymmetric  $P6_3/mmc(00\gamma)0000$ .

The initial solution obtained by charge flipping algorithm is a 3D map of the electrostatic potential (e-map) represented as isosurfaces (**Fig. 3a**).

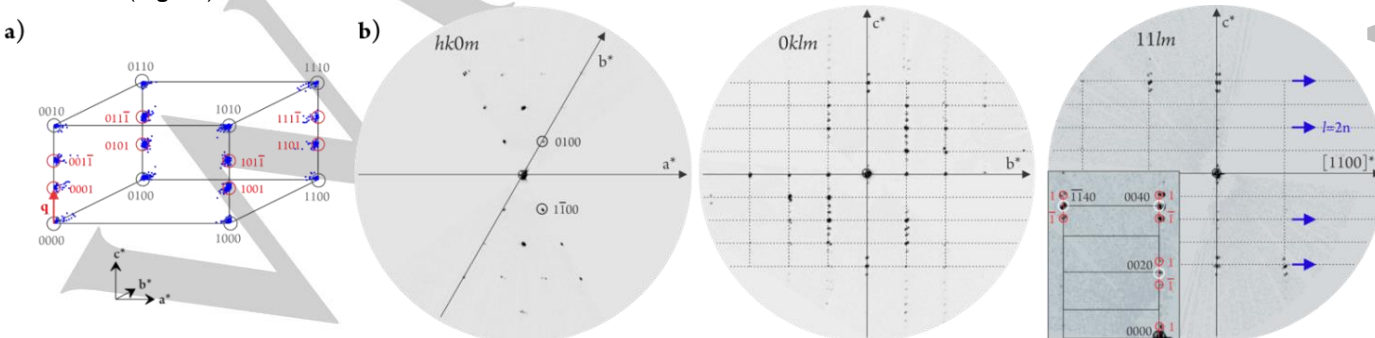


**Figure 2:** a) Reciprocal space projected in one-unit cell showing satellite reflections up to first order (red); b) Sections of reciprocal space from PEDT data

First, the average framework of  $(\text{Mn}, \text{Ni})\text{As}_6$  octahedra is revealed in agreement with the initially reported structure.<sup>[13]</sup> The model is further elaborated by calculating de Wolf sections  $x_3$ - $x_4$  around the two atomic sites corresponding to Mn/Ni and As atoms (**Fig. 3b**). The As site exhibits a displacive modulation along  $c$ , described using a continuous harmonic function. In order to account for the Mn/Ni ordering along [001], the site shared by Mn and Ni atoms is split using discontinuous crenel-like functions associated with one harmonic function.<sup>[18]</sup> Within the resolution of the 3D ED data, the electron scattering amplitudes for Mn and Ni are too close to reliably detect a difference in the electrostatic potential between the domains.

For this reason, the centers of the crenels are set to  $x_4^0(\text{Mn}) = 0.5$  and  $x_4^0(\text{Ni}) = 0$  in order to strain the shortest (longest) distances for Ni-As (Mn-As). The crenel widths were set according to the composition:  $\Delta(\text{Mn}) = 0.6$  and  $\Delta(\text{Ni}) = 0.4$  (**Fig. 3b**). For better visualization of the Mn-Ni stacking sequence, the e-map, as well as the interpreted model, is represented in an averaged supercell  $a \times b \times 4c$ . The main experimental parameters are listed in **Table 1 (SI)**.

The model exhibits the alternation of two types of blocks with variable thickness consisting either of layers of  $\text{MnAs}_6$  octahedra or of layers of  $\text{NiAs}_6$  octahedra. Dynamical refinements were carried out against the 3D ED data.<sup>10,11</sup> The included reflections were chosen following the recommendation by Palatinus *et al.*<sup>[20]</sup>  $R\text{Sg}(\text{max}) = 0.9$ ,  $S(\text{max})g(\text{matrix}) = 0.01 \text{ \AA}^{-1}$ ,  $g(\text{max}) = 1.7 \text{ \AA}^{-1}$ . Because of the rather small unit cell volume and the high symmetry, the  $R\text{Sg}(\text{max})$  was set to a high value to thereby include a sufficiently large number of reflections and maintain a good reflection-to-parameter ratio (**Table 1 (SI)**). The refinement gave reliability factors of  $R/wR(\text{obs/all}) = 13.85\%/14.65\%$  for  $N$  obs/all = 796/1788 [main:  $R/wR(\text{obs}) = 12.67\%/14.28\%$ ; 1. order:  $R/wR(\text{obs}) = 16.24\%/15.75\%$ ].

## COMMUNICATION

This represents a huge improvement compared to what offered in a kinematical refinement [ $R/wR(\text{obs/all}) = 3.18\%/35.39\%$  for  $N_{\text{obs/all}} = 88/128$ ].

The crystal structure of  $\text{Mn}_{0.60}\text{Ni}_{0.40}\text{As}$  exhibits an alternation of 3-4 layers of MnAs and 2-3 layers of NiAs (Fig. 3c), described by a genuine incommensurate modulation with respect to the chemical composition. As shown by Fjellvåg *et al.*<sup>[13]</sup> the  $\text{Mn}_{0.60}\text{Ni}_{0.40}\text{As}$  sample represents just an arbitrary composition for the  $\text{Mn}_{1-x}\text{Ni}_x\text{As}$  solid solution where superstructure peaks are observed. The simulated HAADF image (calculated by JEMS software) based on the aforementioned incommensurate structure model is included in Fig. 1b and shows very good compliance with the observed image. The observed positional modulation of the Mn, Ni and As atoms along [001] dictates a difference in the cell volume for the MnAs and NiAs layers, being in agreement with unit cell volumes of the binary compounds as well as the HAADF images.

The expected Mn-As and Ni-As bond lengths are reached owing to the displacive modulations of As and Mn/Ni along the stacking direction  $c$  (Fig. 3d). This information corroborates our initial observations from HAADF imaging (Fig. 1b and 1c).

The collected powder neutron diffraction (PND) pattern shows intense reflections at low scattering angle (Fig. 4), e.g. at  $0.42 \text{ \AA}^{-1}$ , which is a first-order satellite reflection from the compositional modulation of Mn and Ni. The strong signal of the satellite reflections is a consequence of the excellent contrast between Mn and Ni in PND, due to the different signs of their scattering lengths. Thus, unlike what was feasible with 3D ED data, the sample composition can be determined with accuracy by Rietveld refinement of the crenel widths from PND data. The derived composition of  $\text{Mn}_{0.598(3)}\text{Ni}_{0.402(7)}\text{As}$  is in line with the nominal composition from synthesis.

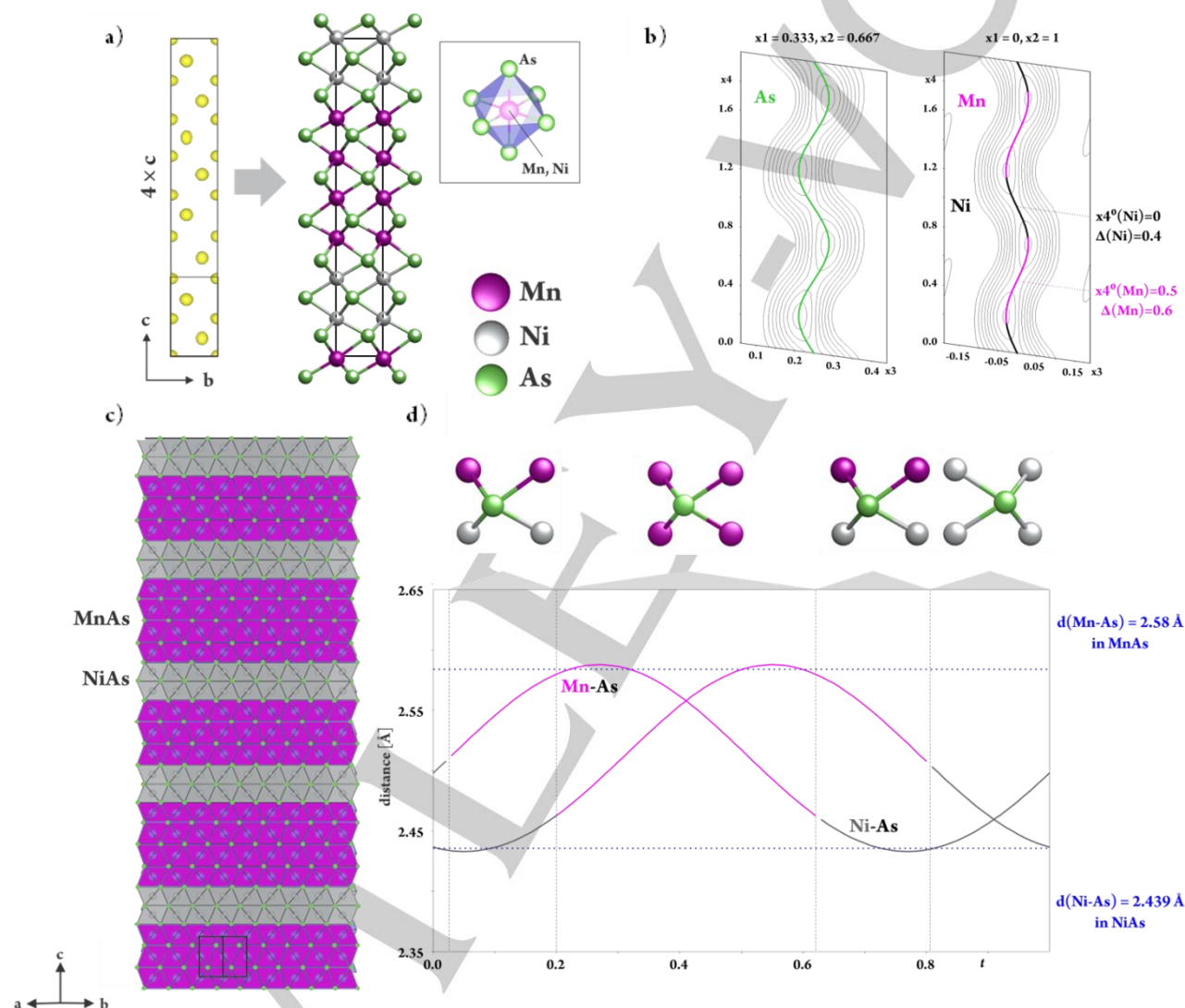


**Figure 3:** a) [100] projection of the 3D electronic potential map and its interpretation as a structural model. For better visualization of the layers, the model is extended along the stacking direction [001]. The Mn and Ni cations are in octahedral coordination; b) On the De Wolf section  $x_3$ - $x_4$  calculated around the As site, the cationic site is described with a continuous harmonic function and split between 2 sites for Mn and Ni using discontinuous crenel-like functions; c) Extended [110] projection of the refined structure against PEDT data (dynamical refinement); d) Variation in Mn - As and Ni - As distances showing the evolution of the local As environment as function of the modulation.

The modulation vector obtained from the PND Rietveld refinements [ $\mathbf{q} = 0.3594(2) \mathbf{c}^*$ ] is identical to that obtained by 3D ED [ $\mathbf{q} = 0.360(3) \mathbf{c}^*$ ]. We note that the results obtained from refinements of PND and 3D ED data are identical, within statistical uncertainty. We emphasize that the combination of PND and 3D ED data was necessary to fully understand the structure as PND is superior for refining the exact composition, while 3D ED was needed for structural determination. The final refined structural model from both data sets is presented in Table 1 and Table 2.

## COMMUNICATION

**Table 1: Unit-cells parameters extracted from refinement of 3D ED data and neutron diffraction data.**

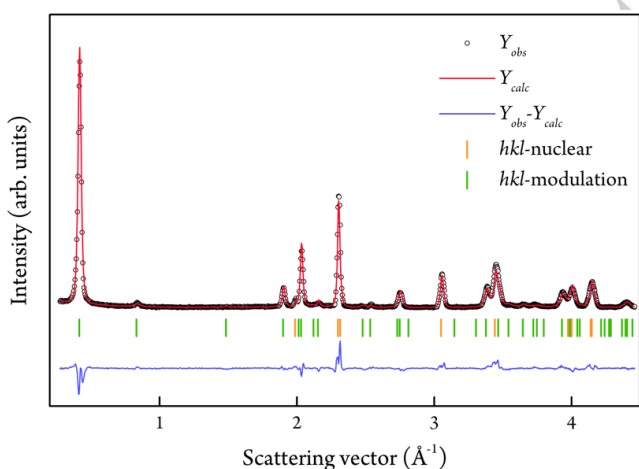
Structural formula	AsMn <sub>0.6</sub> Ni <sub>0.4</sub>
Unit-cell parameters (PEDT)	$a = 3.653(8) \text{ \AA}$ , $c = 5.417(3) \text{ \AA}$ , $\gamma = 120^\circ$ , $q = 0.360(3) c^*$ , $V = 62.67 \text{ \AA}^3$
Unit-cell parameters (NPD)	$a = 3.6520(2) \text{ \AA}$ , $c = 5.4280(6) \text{ \AA}$ , $\gamma = 120^\circ$ , $q = 0.3594(2) c^*$ , $V = 62.694(6) \text{ \AA}^3$
Z	2
Density [g.cm <sup>-3</sup> ] (from NPD)	6.96(7)
Space group	<i>P6<sub>3</sub>/mmc</i>

**Table 2. Positional parameters extracted from the dynamical refinement of 3D ED data and neutron diffraction data.**

Dynamical refinement against 3D ED data							
atom	$\Delta/Occ.$	harm.	$x/a$	$y/b$	$z/c$	$U_{iso} [\text{\AA}^2]$	
Mn1	0.6		0	1	0	0.0191(9)	
		s,1	0	0	-0.0313(6)		
Ni1	0.4		0	1	0	0.0191(9)	
		s,1	0	0	-0.0313(6)		
As1	1		0.3333	0.6667	0.25	0.0215(9)	
		s,1	0	0	-0.0468(6)		
Refined positional parameters (powder neutron)							
Mn1	0.598(3)	s,1	0	0	-0.003(3)	0.016(1)	
Ni1	0.402(3)	s,1	0	0	-0.003(3)	0.016(1)	
As1	1	s,1	0	0	-0.037(1)	0.005	

The type of intrinsic “nano-layering” observed for Mn<sub>0.60</sub>Ni<sub>0.40</sub>As is unique. There exist a few examples of related features. It is reminiscent of the layered ferecrystals that can be described as an intergrowth between two different types of cation - anion layers, bonded by weak Van der Waals forces (e.g. *m* bilayers of SnSe and one trilayer of NbSe<sub>2</sub>, [(SnSe)<sub>1+y</sub>]<sub>*m*</sub>(NbSe<sub>2</sub>)<sub>1</sub>). However, ferecrystals clearly differ from Mn<sub>0.60</sub>Ni<sub>0.40</sub>As by being constructed of weakly bonded building bricks that furthermore can exist as independent well defined compounds.

The present phenomenon is unlike that of other modulated compounds. The layers in the Mn<sub>0.60</sub>Ni<sub>0.40</sub>As compound are of the same crystal structure, in contrast to the Nowotny Chimney-ladder phases. In compounds like Cu<sub>3+x</sub>Si, the modulation is positional and is not originating from an ordering between Cu and Si atoms.

**Figure 4: Experimental (black crosses), calculated (red line) and difference (blue line) neutron powder diffraction pattern of Mn<sub>0.60</sub>Ni<sub>0.40</sub>As according to Rietveld refinement. Main and satellite Bragg peak positions are indicated with green and orange sticks, respectively.**

The oxide LaNb<sub>0.88</sub>W<sub>0.12</sub>O<sub>4.06</sub> has certain similarities to Mn<sub>0.60</sub>Ni<sub>0.40</sub>As by being occupationally modulated. However, there are significant differences: (i) only occupational modulation is observed, while Mn<sub>0.60</sub>Ni<sub>0.40</sub>As exhibits both occupational and positional modulation; (ii) the occupational modulation of Mn and Ni in Mn<sub>0.60</sub>Ni<sub>0.40</sub>As leads to a complete segregation into MnAs and NiAs regions, whereas LaNb<sub>0.88</sub>W<sub>0.12</sub>O<sub>4.06</sub> only shows partial segregation of W; (iii) the architecture of the segregation itself differs; 2D layers versus 3D network, and (iv) the bonding in the two cases is very different; metallic versus polar covalent/ionic. Last, we note that MnAs is ferromagnetic and NiAs is paramagnetic, which makes the intrinsically nanolayered material a potential candidate for spintronics.

**Conclusion**

Mn<sub>0.60</sub>Ni<sub>0.40</sub>As is, to our knowledge, the first example of a representative of a solid solution compound where the chemical composition is directly reflected in an occupational modulation that is intimately coupled to a positional modulation. It is surprising that this exotic and unique phenomenon with Mn-Ni occupational modulation occurs for a phase ideally taking the simple NiAs-type structure. We stress that this modulation of composition, materialized by ultrathin layers consisting of edge- and face-sharing Mn-As octahedra and of Ni-As octahedra, is different from any other stacking or order/disorder phenomena.

The modulated structure is the genuine crystal structure of Mn<sub>0.60</sub>Ni<sub>0.40</sub>As. The periodic variation in the stacking of 2D layers of MnAs and NiAs, creates an incommensurate modulation, with 3-4 thick layers of MnAs and 2-3 layers of NiAs, that in turn determines the chemical composition of the material. In this work, we show how the structural model to describe this peculiar phenomenon can be derived from 3D ED and validated by refinement of powder neutron diffraction data with excellent Mn/Ni scattering contrast. The refined composition is in full compliance with the nominal composition from synthesis. The structure model, as well as the coupled HAADF-EDS mapping images, shows that the MnAs layers have a longer *c*-axis than the NiAs layers, in full agreement with crystallographic data for the individual binary compounds.

We have demonstrated the existence of a fascinating nanophenomenon in a solid-solution phase, and the ability, strength and robustness of state-of-the-art tools in crystallography and methodology to solve and describe complex incommensurate phenomena, all acting as inspiration for future research. The modulated feature of strongly magnetic MnAs and non-magnetic NiAs layers with periodic layer thicknesses at the 1 nm scale, is likely to attract attention in fields like spintronics.

## COMMUNICATION

## References

- [1] J. D. C. McConnell, V. Heine, *Phys. Rev. B* **1985**, *31*, 6140–6142.
- [2] C. J. Howard, M. A. Carpenter, *Acta Cryst B* **2010**, *66*, 40–50.
- [3] L. J. Gillie, J. Hadermann, O. Pérez, C. Martin, M. Hervieu, E. Suard, *Journal of Solid State Chemistry* **2004**, *177*, 3383–3391.
- [4] L. Norén, R. L. Withers, R. Berger, *Journal of Solid State Chemistry* **2000**, *151*, 260–266.
- [5] M. Boström, S. Lidin, *Journal of Alloys and Compounds* **2004**, *376*, 49–57.
- [6] H. Lind, M. Boström, V. Petříček, S. Lidin, *Acta Cryst B* **2003**, *59*, 720–729.
- [7] S. Y. Piao, L. Palatinus, S. Lidin, *Inorg. Chem.* **2008**, *47*, 1079–1086.
- [8] C. Li, S. S. Pramana, S. J. Skinner, *Dalton Trans.* **2019**, *48*, 1633–1646.
- [9] D. C. Fredrickson, S. Lee, R. Hoffmann, *Inorg. Chem.* **2004**, *43*, 6159–6167.
- [10] N. Sato, H. Ouchi, Y. Takagiwa, K. Kimura, *Chem. Mat.* **2016**, *28*, 529–533.
- [11] F. E. Rohrer, H. Lind, L. Eriksson, A.-K. Larsson, S. Lidin, *Zeitschrift für Kristallographie - Crystalline Materials* **2001**, *216*, 190–198.
- [12] L. Palatinus, M. Klementová, V. Dřínek, M. Jarošová, V. Petříček, *Inorg. Chem.* **2011**, *50*, 3743–3751.
- [13] H. Fjellvag, A. Kjekshus, A. Andresen, A. Zieba, *J. Magn. Magn. Mater.* **1986**, *61*, 61–80.
- [14] M. Gemmi, E. Mugnaioli, T. E. Gorelik, U. Kolb, L. Palatinus, P. Boullay, S. Hovmöller, J. P. Abrahams, *ACS Cent. Sci.* **2019**, *5*, 1315–1329.
- [15] G. Steciuk, L. Palatinus, J. Rohlíček, S. Ouhenia, D. Chateigner, *Sci Rep* **2019**, *9*, 9156.
- [16] N. Alsén, *Geologiska Föreningen i Stockholm Förhandlingar* **1925**, *47*, 19–72.
- [17] R. Wilson, J. Kasper, *Acta Crystallographica* **1964**, *17*, 95-.
- [18] V. Petříček, V. Eigner, M. Dušek, A. Čejchan, *Zeitschrift für Kristallographie - Crystalline Materials* **2016**, *231*, 301–312.
- [19] L. Palatinus, V. Petříček, C. A. Corrêa, *Acta Cryst A, Acta Cryst Sect A, Acta Crystallogr A, Acta Crystallogr Sect A, Acta Crystallogr A Cryst Phys Diffr Theor Gen Crystallogr, Acta Crystallogr Sect A Cryst Phys Diffr Theor Gen Crystallogr* **2015**, *71*, 235–244.
- [20] L. Palatinus, C. A. Corrêa, G. Steciuk, D. Jacob, P. Roussel, P. Boullay, M. Klementová, M. Gemmi, J. Kopeček, M. C. Domeneghetti, F. Cámara, V. Petříček, *Acta Crystallogr B Struct Sci Cryst Eng Mater* **2015**, *71*, 740–751.
- [21] L. Palatinus, P. Brázda, M. Jelínek, J. Hrdá, G. Steciuk, M. Klementová, *Acta Crystallogr B Struct Sci Cryst Eng Mater* **2019**, *75*, 512–522.
- [22] L. Palatinus, G. Chapuis, *J Appl Cryst* **2007**, *40*, 786–790.
- [23] “Crystallographic Computing System JANA2006: General features : Zeitschrift für Kristallographie - Crystalline Materials,” can be found under <https://www-degruyter-com.inc.bib.cnrs.fr/view/j/zkri.2014.229.issue-5/zkri-2014-1737/zkri-2014-1737.xml>, **2014**.
- [24] P. Boullay, L. Palatinus, N. Barrier, *Inorg Chem* **2013**, *52*, 6127–6135.
- [25] K. Rickert, P. Boullay, S. Malo, V. Caignaert, K. R. Poeppelmeier, *INORG. CHEM.* **2016**, *55*, 4403–4409.
- [26] G. Steciuk, P. Boullay, A. Pautrat, N. Barrier, V. Caignaert, L. Palatinus, *Inorg. Chem.* **2016**, *55*, 8881–8891.

## Acknowledgments

This work is part of the activities of the NAMM project (Novel Approaches to Magneto-Structural phases transitions in Metallic systems), supported by the Research Council of Norway (Grant no. 263241). Authors want to acknowledge Susmit Kumar, Center for Materials Science and Nanotechnology, Department of Chemistry, University of Oslo for fruitful discussions. The authors acknowledge Vivian Nassif, Inès Puente-Orench and the staff at the D1B beamline, ILL, France, for beamtime allocation and technical support. (S)TEM experiments have been performed in the CRISMAT Lab. (UMR6508, Caen, France) within the frame of the METSA federation (FR3507). G.S. acknowledges the Czech Science Foundation through Project No. 19-07931Y.

## Conflict of Interest

The authors declare no conflict of interest.

**Keywords** Solid-State Structures, Intermetallics, Electron Diffraction, Neutron Diffraction

## COMMUNICATION

## Experimental Section

## Synthesis

The  $\text{Mn}_{0.6}\text{Ni}_{0.4}\text{As}$  compound was synthesized using solid-state reaction. First, MnAs and NiAs binaries were synthesized from stoichiometric amounts of elements Mn, Ni and As, weighed and crushed using agate mortar and pestle. Powders were introduced in alumina crucibles and put into vacuum sealed quartz tubes. Latter were placed in a standing tube furnace and slowly heated up to  $900^\circ\text{C}$  ( $0.1^\circ\text{C}/\text{min}$ ) for a week. Cooling down to room temperature was performed at a  $1^\circ\text{C}/\text{min}$  rate. Ternary compound was prepared weighing stoichiometric amounts of MnAs and NiAs introduced in alumina crucibles, latter placed in quartz tubes, introduced in a standing furnace. Tube was slowly heated ( $1^\circ\text{C}/\text{min}$ ) up to  $800^\circ\text{C}$ , held at this temperature for 5 days and cooled to room temperature at the same rate. This process has been repeated three times with intermediate crushings. Finally, the sample was annealed at  $600^\circ\text{C}$  for 1 month with the same heating and cooling rate.

## Atomic imaging

High-Angle Annular Dark Field (HAADF) imagery imaging was performed on an ARM 200F with a corrected probe, operating at 200kV and equipped with Centurio EDX spectrometer. The simulated ADF images have been calculated with the JEMS software considering the convolution of the STEM probe with the intensity of the object (square of the projected potential multiplied by the electron-matter interaction constant of the structure).

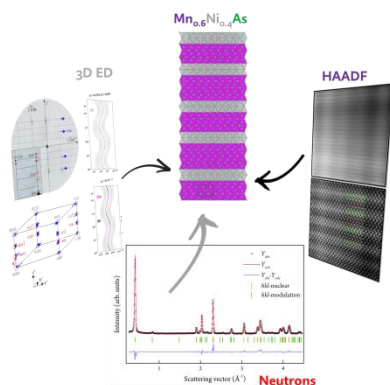
## 3D Electron Diffraction (3D ED)

A small quantity of  $\text{Mn}_{0.6}\text{Ni}_{0.4}\text{As}$  powder ( $<1\ \mu\text{g}$ ) was dispersed in a butanol solution and ground in an agate mortar. A drop of the suspension was deposited and dried on a copper grid with a thin film of holey amorphous carbon. 3D ED experiment was performed with a JEOL 2100 transmission electron microscope (operating at 200 kV with a  $\text{LaB}_6$  cathode) equipped with a Nanomegas DigiStar precession module and a retractile side-entry Gatan ORIUS 200D CCD camera. PEDT data of non-oriented patterns were collected at room temperature. The precession angle was set to  $1.2^\circ$  with a goniometer tilt step below  $1^\circ$ . The PEDT data set was analyzed using the computer programs PETS2.0<sup>[21]</sup>, SUPERFLIP<sup>[22]</sup>, and JANA2006.<sup>[23]</sup> Details about the methodology to solve incommensurately modulated structures using PEDT can be found elsewhere<sup>[12,24–26]</sup>. For each data set, the result is a list of  $hklm$  indices with associated intensities and estimated standard deviations based on counting statistics (Table 1).

## Neutron Diffraction

Neutron powder diffraction (NPD) data has been collected at room temperature on D1B, ILL, France, using wavelength  $\lambda = 2.52\ \text{\AA}$ . About 5 g of the sample was put into a cylindrical vanadium can. Rietveld refinements were carried out in JANA2006.<sup>[23]</sup> The Rietveld refinement resulted in  $R_p = 0.0654$ ,  $wR_p = 0.0894$ ,  $GOF = 0.0334$  and  $R/wR$  (obs) all =  $0.0571/0.0659$  for  $N$  obs/all reflections = 41/44 (main:  $R/wR$ (obs)  $0.0574/0.0571$ ; order 1:  $R/wR$ (obs) =  $0.0401/0.0501$ ; order 2:  $R/wR$ (obs) =  $0.1229/0.1171$ ) (see refinement details in Table 1). Data are found at <http://doi.ill.fr/10.5291/ILL-DATA.DIR-172>

## COMMUNICATION



In this paper, we unravel a structural feature that has remained unsolved for decades. We unveil an incommensurate occupational modulation which creates a particular nanoscale ordering of MnAs and NiAs layers in the intermetallic  $\text{Mn}_{0.60}\text{Ni}_{0.40}\text{As}$  solid solution phase. We have investigated this extraordinary phenomenon by *state-of-the-art* methodology; 3D electron diffraction (PEDT), high-angle annular dark-field (HAADF) imaging, and neutron diffraction.